Check for updates

The FEBS Journal

FEBS PRESS science publishing by scientists

Motif-driven protein binder design towards transferrin receptor helical domain

Dick J. Sjöström[1], Camilla Mohlin[1], Elena Ambrosetti[2], Scott J. Garforth[3], Ana I. Teixeira[2] and Sinisa Bjelic[1]

1 Department of Chemistry and Biomedical Sciences, Linnaeus University, Kalmar, Sweden
2 Department of Medical Biochemistry and Biophysics, Karolinska Institutet, Stockholm, Sweden
3 Department of Biochemistry, Albert Einstein College of Medicine, Bronx, NY, USA

Keywords
protein design; ROSETTA; transferrin receptor; yeast surface display

Correspondence
S. Bjelic, Department of Chemistry and Biomedical Sciences, Linnaeus University, Kalmar, Sweden
Tel: +46 480 44 62 64
E-mail: Sinisa.Bjelic@lnu.se

(Received 24 June 2021, revised 29 October 2021, accepted 2 December 2021)

doi:10.1111/febs.16311

Human transferrin receptor 1 (TfR) is necessary for the delivery of the iron carrier protein transferrin into cells and can be utilized for targeted delivery across cellular membranes. Binding of transferrin to the receptor is regulated by hereditary hemochromatosis protein (HFE), an iron regulatory protein that partly shares a binding site with transferrin on TfR. Here, we derived essential binding interactions from HFE and computationally grafted these into a library of small protein scaffolds. One of the designed proteins, TB08, was further optimized computationally and experimentally to identify variants with improved binding to TfR. The optimized variant, TB08 S3.1, expressed well in the *E. coli* expression system and had an affinity to TfR in the low micromolar range, $K_d \approx 1$ μM, as determined by surface plasmon resonance. A binding competition assay with transferrin further confirmed the interaction of the evolved variant to TfR at the shared binding surface. Additionally, the GFP-tagged evolved variant of TB08 demonstrated cellular internalization as determined by fluorescent and confocal microscopy in HeLa cells. The designed protein is small, allows for robust cargo tagging, and interacts specifically with TfR, thus making it a valuable tool for the characterization of TfR-mediated cellular transport mechanisms and for the assessment of engineering strategies for cargo delivery across cell membranes.

Introduction

Transport of iron ions in the blood stream is achieved by the protein carrier transferrin (Tf) [1]. Upon binding of transferrin to its cellular receptor, namely transferrin receptor 1 (TfR), the complex gets internalized where acidic conditions of the endosome lead to the release of iron from transferrin [2]. At the end of the endocytic cycle, the apo Tf remains bound to the receptor and most of the complexes get recycled to the cell surface where physiological pH leads to Tf dissociation and release into the blood stream after which the process of iron delivery is repeated. In addition to Tf, TfR can bind hereditary hemochromatosis protein (HFE) and ferritin, which is also followed by internalization of the complexes. The internalization of proteins via TfR is explored for biomedical applications, and several studies have been reported to ferry engineered peptides and protein variants across cellular membranes [3–8]. From a structural perspective, TfR is a dimeric transmembrane protein with a large ectodomain, therefore, presenting a large binding surface area for non-native molecular interactions [9]. The receptor monomer is built from the helical, protease-like, and apical domains where each domain can be roughly assigned a certain task. The helical domain is

Abbreviations
HFE, hereditary hemochromatosis protein; MFU, mean fluorescence units; Tf, transferrin; TfR, transferrin receptor 1.

This is an open access article under the terms of the Creative Commons Attribution-NonCommercial-NoDerivs License, which permits use and distribution in any medium, provided the original work is properly cited, the use is non-commercial and no modifications or adaptations are made.

responsible for the dimerization and binding of endogenous ligands transferrin [10] and HFE [11], where the iron delivery via Tf–TfR complex is regulated by HFE because of directly overlapping binding sites on the receptor, thus leading to the lower affinity for iron-loaded Tf in the presence of the bound HFE (1 : 1 : 1 ration of HFE–TfR–Tf) [12,13]. Recent evidence has suggested that TfR is constitutively internalized independently of any protein ligand bound [14], therefore, lending itself for exploitation by exogenous binders. Specifically, the apical domain is preferred for interactions by pathogens to gain cellular entry, for example, both viral glycoproteins [15] and the malarial protein *Pv*RBPv2 [16] interact with the apical domain. There is furthermore structural evidence that the iron carrier ferritin binds as well to the apical domain [17], besides the pathogenic binders. The protease domain, besides its major contribution to driving the receptor dimerization, is known to interact with *Pv*RBPv2. Hence, independent of the interaction origin, binding to the different domain surfaces on TfR results in cell internalization of the formed complex by endocytosis.

The importance of the Tf–TfR complex in physiology, and its significance in biomedicine, both as a therapeutic target and as a vehicle for therapeutic delivery, has garnered significant interest in the development of novel strategies to engineer binders that interact with the receptor [18]. These include short peptides [4], scFVs fused to therapeutics [8], Fc domains of antibodies [3], affibody coupled antibodies [5], and gold nanoparticles coated with Tf [7] or coupled with anti-TfR specific antibodies [19]. The receptor itself has in addition been subjected to protein engineering efforts in which the apical domain had been decoupled from the receptor and expressed as a soluble standalone protein [3,20,21]. A variety of methods have been used to build TfR binders, including computational design strategies [6]. The prevalent approach has utilized selection from a library of potential protein binders. The resulting TfR binders from these applications are generally not aimed at a predefined surface on the receptor but fulfill the overall goal of achieving specific interactions. Additionally, these studies have been focused almost exclusively on antibody development. To further advance the study of TfR biology and develop therapeutic applications of TfR targeting, it would be beneficial to control the targeted surface and to build binders that interact with specific areas of the receptor. Computational methods have made such developments increasingly possible and have been used to make binders based on optimizing the placement of specific hydrophobic amino acids at the desired interacting surface and grafting these into scaffold proteins [22], grafted secondary structure elements [23,24], and de novo designed miniproteins not derived from antibodies or their domains [6].

Since the large, exposed surface of the transferrin receptor makes it well suited for binding of protein molecules and the receptor can be internalized by endocytosis, it is suitable for the development of computationally engineered protein binders that target specific areas on the receptor. Here, we mainly focus on the helical domain to design such protein binders. While both Tf and HFE target the overlapping interaction surfaces of the helical domain, they are large proteins and transferrin additionally contains the iron-binding sites. The designed proteins we present here are built from protein scaffolds that are restricted to smaller size. This methodology allows us to control on the atomic level the binding interface and its localization on the transferrin receptor, providing a straightforward strategy for optimization of biochemical properties. Here, we present a computationally designed protein that has its interactions derived from HFE and therefore targets the helical domain of TfR, partially sharing the binding surface of the receptor with both endogenous transferrin and HFE. Although the evolved variant binds to TfR with a dissociation constant (K_d) in the low micromolar range, it is a promising starting point for further sequence optimization and structural diversification for the study of TfR-mediated endocytosis or biomedical applications in which cellular internalization is required.

Results and discussion

We applied a computational methodology that allowed us to graft the naturally occurring hotspot interactions from HFE protein into a small scaffold protein (Fig. S1). The helix containing the HFE hotspots was grafted into the scaffolds from the PDB using ROSETTA software. We tested different lengths of the helix, which resulted in a different number of found scaffolds that were able to accommodate grafts, called matches. In total, 1070 matches were identified in 214 scaffolds, with shorter helices giving a larger number of solutions: 25, 23, 19, and 16 aa segments gave rise to 20, 35, 165, and 850, matches in total, respectively. The probability of finding a match for a shorter helix is higher because of the larger number of possibilities of placing such segment in a scaffold, which gives rise to higher number of solutions. Therefore, the 25 aa segment was successfully placed only in 4 scaffolds, while the 16 aa segment gave solutions in 170 scaffolds. The total number of matches was thus proportional to the number of scaffolds with possible solutions. After

17424658, 2022, 10, Downloaded from https://febs.onlinelibrary.wiley.com/doi/10.1111/febs.16311 by Elena Ambrosetti - CochraneItalia , Wiley Online Library on [08/11/2025]. See the Terms and Conditions (https://onlinelibrary.wiley.com/terms-and-conditions) on Wiley Online Library for rules of use; OA articles are governed by the applicable Creative Commons License

sequence optimization of the scaffolds, designs were sorted by shape complementarity greater than 0.55 and by interface surface area greater than 1000 Å^2, which gave 40 designs for further optimization in which reversions were made with respect to the native or homologue sequences.

The explored computational design strategy against TfR used grafting of secondary structure elements containing the hotspot residues, thus using the interactions that were naturally evolved. The methodology gave designs that were made specifically toward the helical domain of the receptor. The recently published work by Sahtoe *et al.* [6] explored an alternative design strategy to target the exposed beta strand edge of the TfR apical domain. This was accomplished by designing interacting beta strands and grafting these in the set of protein scaffolds. While there are similarities shared between the methods, like grafting the secondary structures in scaffolds, the latter method is both more general but also more demanding in terms of computational modeling. Nevertheless, these methods gave solutions that were steered toward different domains of the receptor, demonstrating the potential of computational protein design in engineering protein binders targeting desired interacting surfaces.

The designs were visually inspected, and 11 were ordered and tested by YSD and flow cytometry. Out of these, only TB08 showed a shift toward increased binding signal at 1 μM concertation of the target transferrin receptor (Fig. S2, left panel). The TB08 protein scaffold was based on the engineered ribosomal protein S6 from *Thermus thermophilus* deposited with PDB ID 3zzp [25] that consisted of three anti-parallel β-strands, an alpha-helix connecting the β-strands 1 and 3, and an additional C-terminal α-helix (Fig. 1A). The two helices formed the interface to TfR, with the hotspot residues grafted in the C-terminal helix. Consequently, the predicted positioning of the TB08 helices is aligned longitudinally with the TfR helical domain mirroring the orientation of HFE (Fig. S1). The root mean square deviation (RMSD) for superimposed C_α atoms between the grafted helix in the scaffold protein after structure optimization and the corresponding segment in HFE was 0.35 Å. The sequence of the grafted segment was K GAQHE KEVIQ WTIEE in comparison to the native sequence K GWDHM FTVDF WTIME. The residues forming the interface with the receptor were retained during the designed process including the hotspot interactions, V78 and W81 (HFE numbering). In total, there were six grafted residues including the hotspots that are within the interacting distance from TfR: Lys^{70}, His^{74}, Val^{78}, Trp^{81}, Thr^{82}, and Glu^{85}. These closely

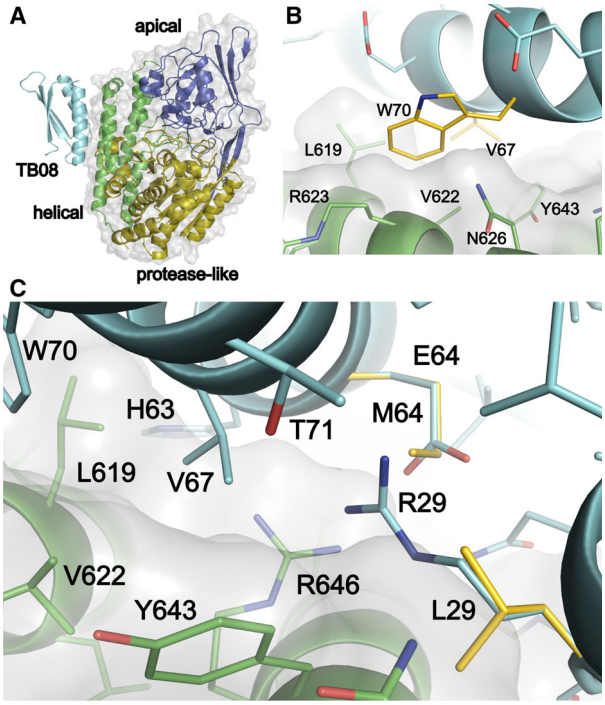

Fig. 1. Interface interactions between the designed protein and TfR (receptor structure and numbering according to PDB ID 1de4). (A) Designed protein TB08 (teal) in the modeled conformation with TfR interacted with the receptor helical domain (green). Also denoted are the apical domain (blue) and protease-like domain (yellow). (B) The grafted Trp^{81} and Val^{78} hydrophobic hotspot anchors of HFE, here shown within the interface between designed TB08 residues Trp^{70} and Val^{67} (yellow) and TfR. Trp^{70} of TB08 formed largely hydrophobic interactions with TfR, specifically with Leu^{619}, Val^{622}, and the methylene groups of Arg^{623}. TB08 Val^{67} forms also hydrophobic interactions with TfR Leu^{619}, Val^{622}, and Tyr^{643}. (C) In addition, in TB08dm, R29L and E64M mutations are shown (yellow); these remove the charged residues in favor for hydrophobic ones at the core of the designed protein. Images were generated with PYMOL.

recapitulate interactions in the native HFE–TfR complex. In addition, Gly^{71} and Ile^{83} were also unchanged in the grafted helix; however, these do not contribute to the interface interactions. The hotspots form a hydrophobic anchor with the alpha-helices of TfR where the indole group is in the contact with the side-chains of Leu^{619}, Val^{622}, and the hydrophobic part of the Arg^{623} side chain (Fig. 1B). On the opposite side from the interface-forming surface, the sequence in the grafted helix was redesigned to allow for better interactions with the core residues in the scaffold protein. Visual inspection of the TB08–TfR complex revealed a designed salt bridge formed in between TB08 residues Arg^{29} and Glu^{64}; the glutamate was also at the interacting distance to the charged guanidium group of TfR Arg^{646} (Fig. 1C). Since the formation of the

17424658, 2022, 10, Downloaded from https://febs.onlinelibrary.wiley.com/doi/10.1111/febs.16311 by Elena Ambrosetti - Cochraneltalia , Wiley Online Library on [08/11/2025]. See the Terms and Conditions (https://onlinelibrary.wiley.com/terms-and-conditions) on Wiley Online Library for rules of use; OA articles are governed by the applicable Creative Commons License

charged–charged residue network was more favorable during the design process, the charged amino acids were incorporated into TB08 structure. In general, the contribution of such charged interactions to the folded structure is difficult to quantify theoretically; therefore, alternative possibilities were investigated by allowing ROSETTA remodel application [26] to sequence optimize only these positions. This led to redesign of the TB08 salt bridge into hydrophobic interactions: R29L and E64M (Fig. 1B).

The designed protein with the double mutation, TB08dm, showed increased binding signal at 1 μM TfR concentration (Fig. S2, Fig. 2A, Table S1) and was used for subsequent sequence optimization of yeast surface displayed variants by FACS. With error-prone mutagenesis, a library of 2×10^6 TB08dm variants was made with an average of 2 mutations per gene, and FACS sorted by three rounds at 1 μM TfR concentration (Fig. 2B). The evolved variants were sequenced and characterized by flow cytometry (Fig. 2C). S3.1 (E47V/I72V/E74D/A75V) and S3.8 (N20Y/R27C/R34C/M36I/P43S/N49Y/I68F) showed a higher signal than the remaining variants, followed by S3.2 (T7P/N20I/N31Y/P43T), S3.3 (Q4L/N20I/N31Y/R34C/A39S/K59N) and S3.4 (M14V/R27C/R34C/Y46F/E47V). S3.5 (N49D) also showed initially a higher-binding signal than TB08dm (Table S1). TfR-mediated transport across the blood–brain barrier for antibodies demonstrated that tighter binding may not be desirable as it may lead to less optimal transcytosis [27]. Yu *et al* showed that IC50 = 111 nM of Ab binding to TfR resulted in the highest brain uptake in comparison to tighter binding variants. Following that hypothesis, we decided to stop evolving our library as soon as we got a binder with $K_d \approx 1$ μM. Since the mutagenesis rate after sorting was high, single residue mutations were incorporated into TB08dm to assess whether they individually have any significant contribution to binding. The variants with a binding signal higher than TB08dm, Q4L and R34C, were further characterized by incorporating them alone or in combination into the S3.1 variant. However, the combinations did not lead to any markedly improved binding. Decomposition of individual mutations and in combination was furthermore assessed for the S3.1 variant. The single, double, and triple mutations lead to higher binding, but none of the combined mutations reached up to the signal of S3.1 variant in the YSD system (Fig. 3).

To validate the binding, we carried out SPR-binding assays for the TB08, TB08 S3.1, and TB08 S3.1–sGFP variants as the evolved variant consistently showed better binding in the YSD system. First, we expressed these variants in bacteria and purified the proteins with immobilized metal affinity chromatography. The purification procedure resulted in high production yields, of approximately 25 mg, 13 mg, and 3.5 mg, purified protein for TB08, TB08 S3.1, and TB08 S3.1–sGFP, respectively, when expressed in a 0.5 L culture. The binding of the TB08 S3.1 variant to TfR was determined by SPR after immobilizing the biotinylated receptor to the streptavidin sensor chip. The K_d values determined for TB08 S3.1 and TB08 S3.1-sGFP were 1.1 μM and 3.7 μM, respectively (Fig. 4A), in agreement with the apparent YSD-binding signal. TB08, tested at the same concentrations, showed a minimal SPR-binding signal, indicating that the K_d falls in the high-micromolar/millimolar range. In parallel, as positive control, we determined the binding of transferrin to the TfR and obtained K_d = 56.1 nM (Fig. S3). Furthermore, we analyzed the binding of TB08 and TB08 S3.1 to TfR that was chemically immobilized via amine coupling onto the SPR chip. For TB08 S3.1, the dissociation constant was determined to be approximately 20 μM, while for the original design (TB08), it was above the mM detection limit (Fig. S4A). The shift in K_d to higher values in these conditions is likely because of the random amine coupling of lysines of the TfR to the SPR chip. In addition, we determined the apparent dissociation constant for TB08 S3.1 by YSD and titrating the TfR (Fig. S4B). The obtained apparent K_d value of 1.2 μM was in accordance with the measurements of biotinylated-TfR immobilized on the streptavidin-SPR chip indicating the advantage of site-specific coupling. In sum, these results confirm that TB08 S3.1 showed a significantly higher-binding affinity to TfR compared with TB08. Further, the TB08 S3.1 variant did not show any non-specific binding to a control receptor, Her3, immobilized through the amine coupling approach to the SPR chip instead of TfR (Fig. S5).

Yeast-displayed TB08 S3.1 was tested in a competition assay with 1 μM Tf, keeping the receptor concentration at 1 μM (Fig. S6). The binding signal was reduced by 55% for TB08 S3.1, indicating an overlapping binding site to TfR. Similarly, TB08 S3.1 bacterially purified protein was tested in competition with yeast displayed TB08 S3.1; 4 μM of TB08 S3.1 bound to 1 μM TfR, representing a 70% reduction in the binding signal (Fig. S7). The SPR-binding assays together with the competition assays confirmed that the TB08 S3.1 variant bound specifically to the TfR and that the interface overlapped with the Tf-binding surface on the receptor.

The sequence alignment of TB08dm and TB08 S3.1 revealed four mutations E47V, I72V, E74D, and A75V

17424658, 2022, 10, Downloaded from https://febs.onlinelibrary.wiley.com/doi/10.1111/febs.16311 by Elena Ambrosetti - CochraneItalia , Wiley Online Library on [08/11/2025]. See the Terms and Conditions (https://onlinelibrary.wiley.com/terms-and-conditions) on Wiley Online Library for rules of use; OA articles are governed by the applicable Creative Commons License

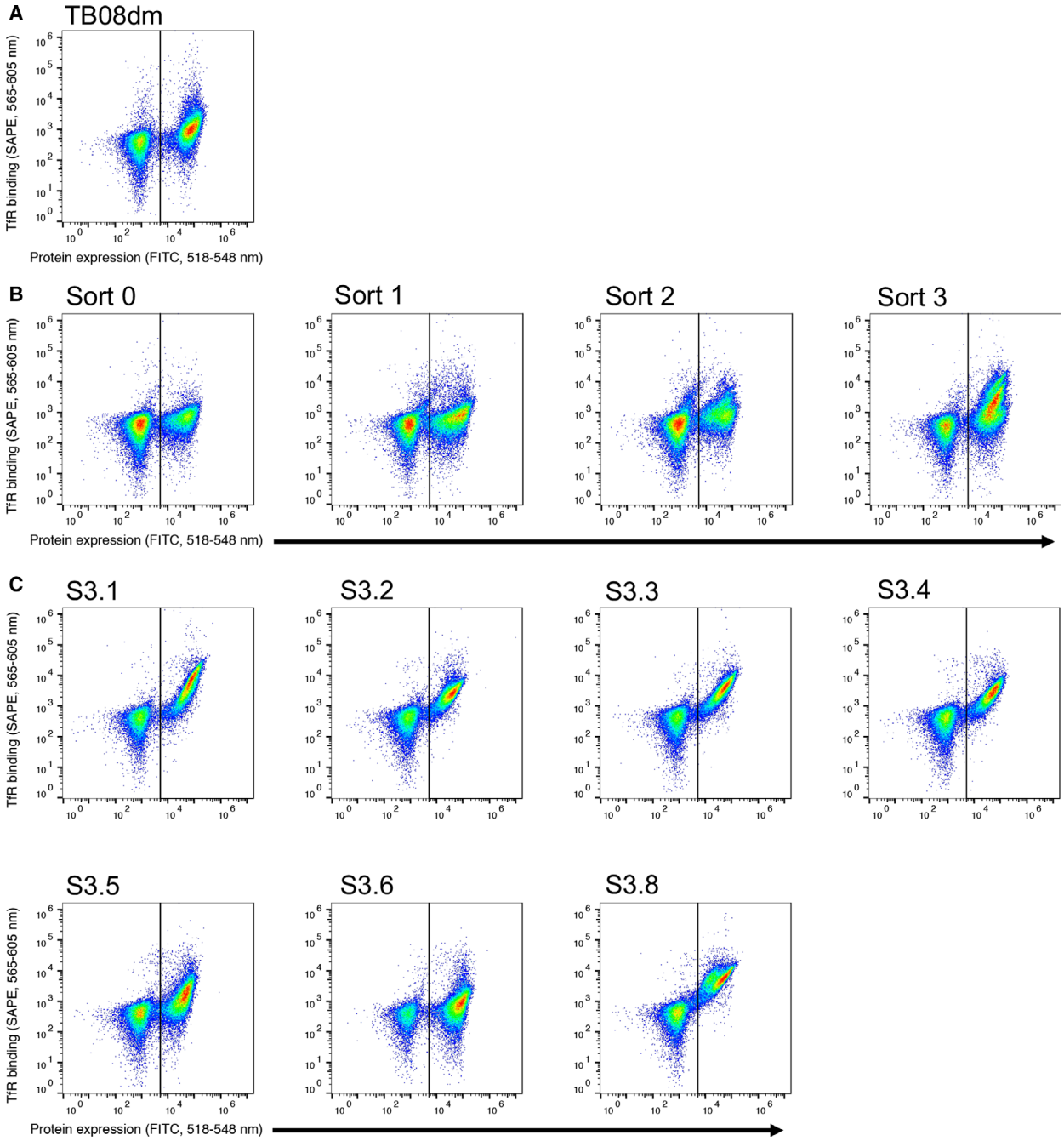

Fig. 2. Flow cytometry characterization of FACS sort rounds and the variants found in sort 3. (A) TB08dm shows a distinct binding signal along the ordinate for the yeast expressing population plotted on the abscissa. (B) FACS sorting of the TB08 library was performed for three rounds Sort 1-3. (C) Tested evolved variants from FACS sort 3 show improved binding signal. In each plot, 50 000 singlet cells were assayed, where protein surface expression is detected by anti-cmyc FITC antibody and binding is detected by SAPE. The assay was performed at 1 μM biotinylated TfR.

introduced after selection (Fig. 4B). The last three mutations were on the grafted helix only 2 and 5 amino acids downstream of the hotspot residues, while the E47V was situated on the beta strand found on the opposite side of the interface. The change of the glutamate to aspartate positions the negative charge close to the ideal hydrogen-bonding distance of the Arg^{629} in the transferrin receptor (3.0 Å, Fig. 4B). It is likely

17424658, 2022, 10, Downloaded from https://febs.onlinelibrary.wiley.com/doi/10.1111/febs.16311 by Elena Ambrosetti - CochraneItalia , Wiley Online Library on [08/11/2025]. See the Terms and Conditions (https://onlinelibrary.wiley.com/terms-and-conditions) on Wiley Online Library for rules of use; OA articles are governed by the applicable Creative Commons License

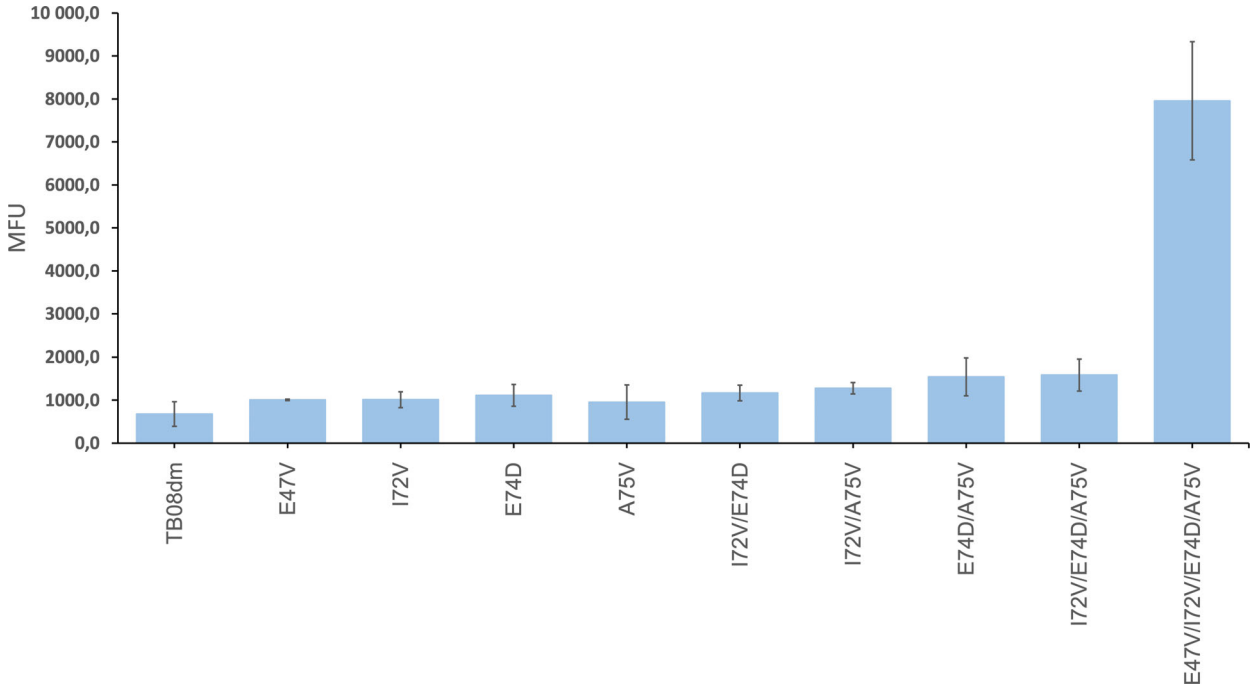

Fig. 3. Flow cytometry measurements of 50 000 fluorescently labeled yeast cells expressing different variants of TB08dm at 1 μM TfR. Both single mutations and their combinations improved binding. Standard deviation, shown as error bars, was calculated from at least two samples.

that the hydrophobic mutations at the positions 72 and 75 fine-adjust the interactions between the Asp–Arg salt bridge, but we cannot exclude that a better positioning of the hotspot residues is achieved simultaneously. These three mutations are located close to the C-terminal and thus close to the His-tag. Although the E47V mutation was located on the opposite face of the complex-forming surface, it is in the beta sheet. This mutation, together with the three other mutations in S3.1, seemed to tune the conformation of TB08 S3.1 leading to better interface formation with the target receptor. To test whether sequence changes between TB08 and TB08 S3.1 contribute to stability instead of structurally fine tuning the evolved protein and thus the interface, we carried out circular dichroism (CD) measurements. The CD spectra indicate well-folded proteins (Fig. S8A) with similar temperature denaturation profiles (Fig. S8B). Any influence of the C-terminally situated His-tag is unlikely, as insertion of the GFP protein in between the TB08 and the His-tag resulted in almost unaffected K_d values, 1.1 μM vs 3.7 μM (Fig. 4A). The SDS–PAGE estimate of the immobilized metal affinity chromatography (IMAC) purified GFP tagged S3.1 variant and the subsequent size exclusion chromatograph (SEC) of the bound fractions eluted as a single monodisperse peak at correct size of approximately 40 kDa, which agreed with its calculated molecular weight $MW_{TB08\ S3.1–sGFP}$ = 38 kDa (Fig. S8C,D). When compared with the HFE protein, the grafted helix in the scaffold aligned with the axis of the native protein as would be expected because of the design strategy (Fig. 4C). As can be seen from Fig. 4C, the side chains of the grafted helix were conserved toward the interacting surface of the receptor, while sequence optimization was necessary toward the core of the protein to accommodate the new interactions. Moreover, the published dissociation constants for HFE binding to the immobilized TfR on a sensor chip are in the order of $K_d \approx 60$ nM (average of published data for K_{d1} = 24 nM and K_{d1} = 98 nM [12,13]). The evolved variant TB08 S3.1 thus captures a significant portion of the binding potential from HFE. The scaffold used for the grafting has been shown to be sensitive to structural adjustments upon mutations, for example, there were small shifts occurring between helices [25], which may explain the improvements in binding during selection with possibly presenting even a higher, unexplored optimization potential. Together, these results show that although the designed protein is much smaller than the native HFE, 80 in comparison to 350 amino acids,

17424658, 2022, 10, Downloaded from https://febs.onlinelibrary.wiley.com/doi/10.1111/febs.16311 by Elena Ambrosetti - CochraneItalia , Wiley Online Library on [08/11/2025]. See the Terms and Conditions (https://onlinelibrary.wiley.com/terms-and-conditions) on Wiley Online Library for rules of use; OA articles are governed by the applicable Creative Commons License

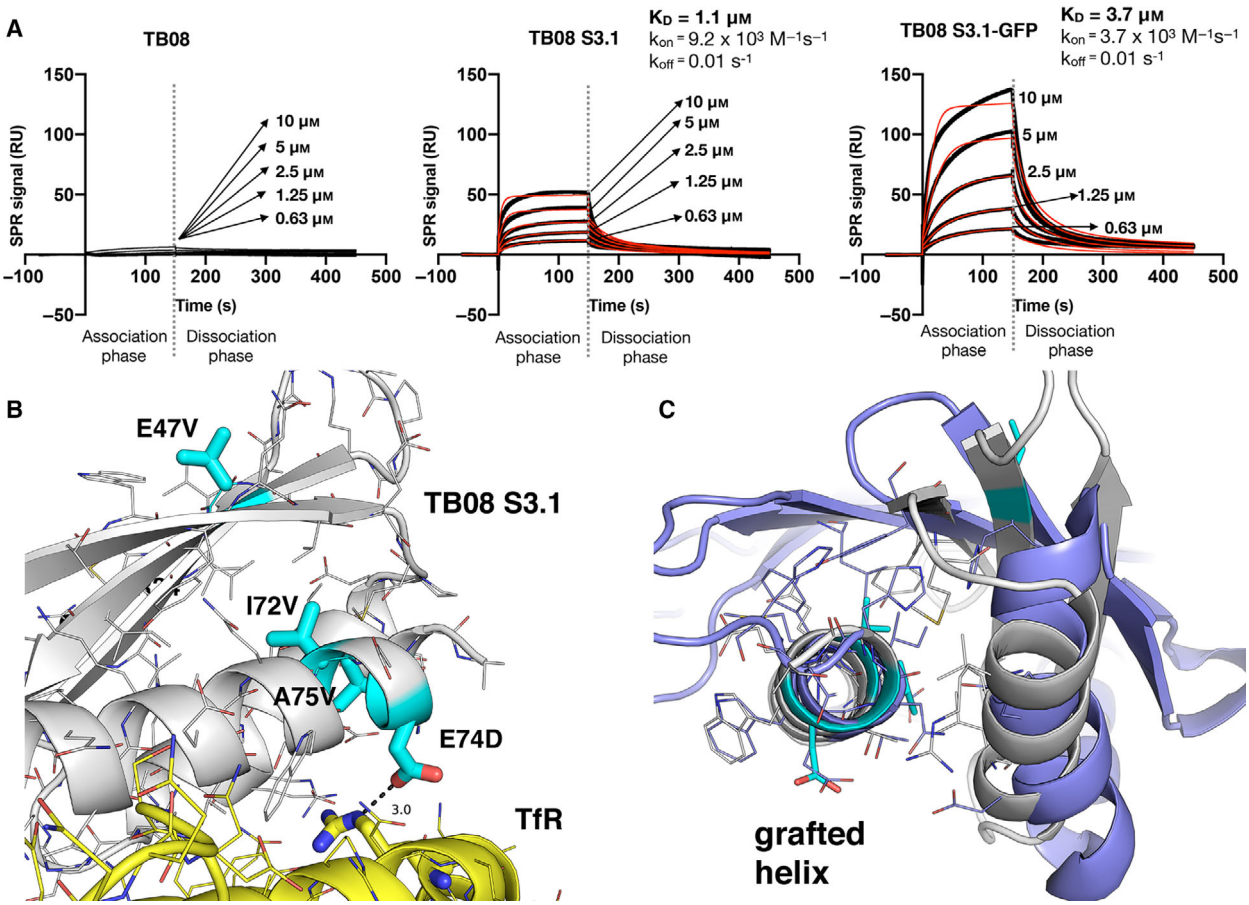

Fig. 4. *In vitro* characterization of the engineered proteins. (A) *In vitro* SPR binding measurement of the bacterially purified TB08 and S3.1 confirmed the improved binding for the evolved variant. The dissociation constant for S3.1 was determined to be 1.1 μM (for the TB08, the dissociation constant could not be determined as it was in mM range). The sGFP-tagged evolved variant, TB08 S3.1-GFP, had a dissociation constant of 3.7 μM, which agreed with the binding of the untagged protein. Recorded sensorgrams are shown in black, while fitting curves are in red. (B) The model of the evolved variant in complex with TfR. There are four mutations in the evolved variant S3.1 compared with the TB08dm that together give the increased binding signal compared with TB08dm. The evolved mutations are shown in cyan; the designed protein in gray; TfR in yellow. (C) The grafted helix from HFE, with retained side chain orientations during the design process, shown here along its axis. The designed protein model in gray; HFE in blue. Images in panels b and c were generated with PYMOL.

respectively, it can accommodate the hotspot residues required for the interaction with the target receptor and lends itself to directed evolution.

To assess TB08 S3.1-sGFP binding to the TfR in the cell membrane and internalization of the resulting protein complex, we treated HeLa cells with 4 μM of TB08 S3.1–sGFP, 4 μM sGFP, or 160 nM Tf chemically coupled to FITC (Tf–FITC). HeLa cells have been shown to express about ~ 10^5 TfR molecules on the cell surface [28]. After incubation with the fluorescently tagged proteins, cells were analyzed using microscopy or flow cytometry. Cells treated with the designed protein TB08 S3.1–sGFP or the positive control Tf-FITC, together with DAPI, were highly fluorescent as determined by flow cytometry in comparison with the negative control consisting of cells treated with DAPI alone (Fig. 5A). The fluorescent signal was about 70 000 mean fluorescence units (MFU) for cells treated with the fluorescently labeled proteins compared with about 4000 MFU for control cells. Fluorescence was distinctively visible on the cell surface when examined in the fluorescence microscope and localized around the DAPI-labeled nucleus (Fig. 5B). Cell viability was unaffected by incubation of TB08 S3.1 while sGFP showed a small decrease, 95% and 83%, respectively. Ten times lower concentration of sGFP, 0.4 μM, did not affect cell viability. There was no indication of any formed aggregates neither for Tf nor for TB08 S3.1-

17424658, 2022, 10, Downloaded from https://febs.onlinelibrary.wiley.com/doi/10.1111/febs.16311 by Elena Ambrosetti - CochraneItalia , Wiley Online Library on [08/11/2025]. See the Terms and Conditions (https://onlinelibrary.wiley.com/terms-and-conditions) on Wiley Online Library for rules of use; OA articles are governed by the applicable Creative Commons License

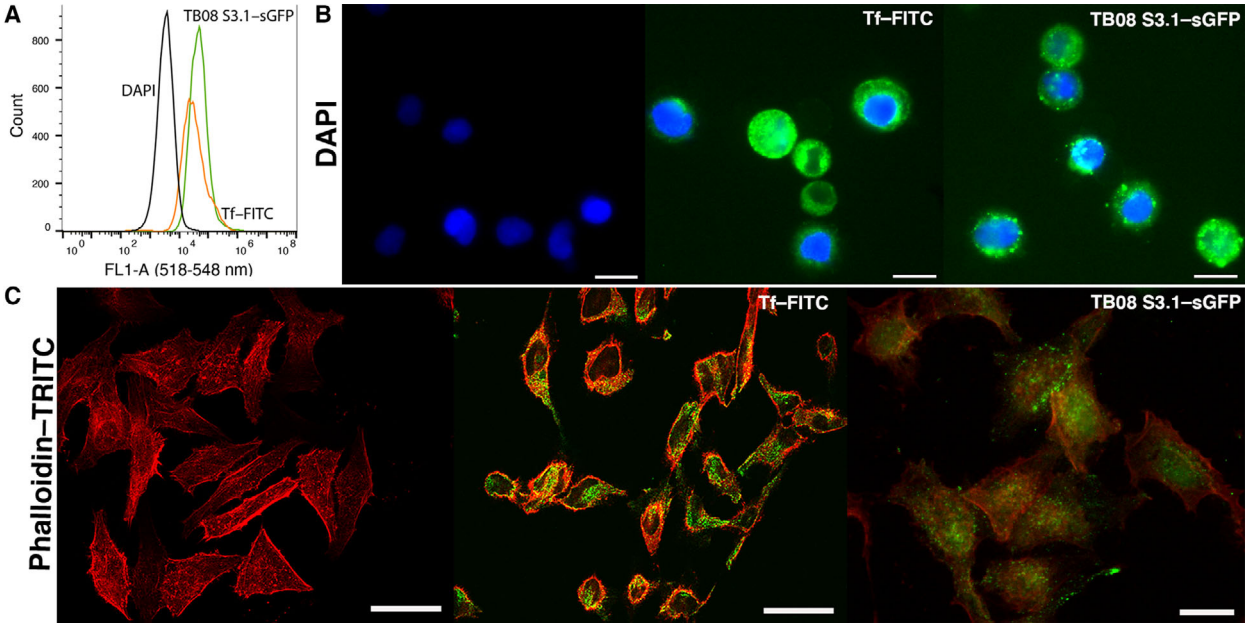

Fig. 5. Analysis of TB08 S3.1 binding to HeLa cells, with DAPI staining as the negative control and Tf–FITC labeling as the positive control. (A) Flow cytometry assay of HeLa cells after incubation with DAPI and Tf–FITC or TB08 S3.1–sGFP demonstrated binding of TB08 variant to the cells because of the clear increase in fluorescence signal compared with the negative control. DAPI showed only background fluorescence (MFU = 4 000); both Tf–FITC and TB08 had a MFU signal of about 70 000. (B) Fluorescence microscopy images of the corresponding HeLa cells agreed with the flow cytometry data, with fluorescently tagged proteins, Tf and TB08, interacting with HeLa cells. The bar indicates 20 μm. (C) Confocal microscopy images of Hela cells labeled with phalloidin-TRITC and Tf–FITC or TB08 S3.1–sGFP indicate that the cells internalized both Tf and TB08 proteins. The bar indicates 20 μm.

treated cells. To investigate whether TB08 S3.1 gets internalized by HeLa cells, confocal microscopy of phalloidin-TRITC and Tf–FITC or TB08 S3.1–sGFP-labeled cells was determined. In both cases, the proteins internalized into cells as simultaneously visualized with actin-bound phalloidin-TRITC (Fig. 5C; Fig. S9 and Fig. S10), indicating that the endocytic mechanism was the most probable pathway for protein uptake. To further investigate the endocytic mechanism of protein uptake within HeLa cells, the assay was additionally carried out at 4 °C in addition to 37 °C with either Tf–FITC or TB08 S3.1–sGFP (Fig. S11). Endocytosis is inhibited at lower temperatures, and temperature reduction has been used as a proof-of-concept in the peptide-based studies of cellular uptake [29,30]. Therefore, decreasing the temperature should lead to the lowering of the fluorescent signal, specifically when measurements are carried out at 4 °C compared with 37 °C. As predicted, we observed a reduced fluorescence signal measured by flow cytometry for HeLa cells incubated with Tf–FITC or TB08 S3.1–sGFP at 4 °C (Fig. S11). Additionally, experiments with HeLa cells, where we titrated TB08 S3.1–sGFP, showed a signal in accordance with dose–response model (Fig. S12). Negative controls, 3zzp–sGFP and sGFP, displayed a significantly lower signal than TB08 S3.1–sGFP when assayed with HeLa cells at 400 nM protein concentration (Fig. S13). Therefore, internalization of sGFP tag within cells demonstrated that even relatively large cargo associated with TB08 S3.1 (sGFP ~ 25 kDa) was endocytosed via TfR-mediated pathway, indicating potential for coupling other cargo molecules for cell delivery.

Conclusions

We have shown that a computationally designed, evolved protein variant, TB08 S3.1, containing the grafted hotspot interactions from HFE binds to TfR at an interface that overlaps with the Tf–TfR binding interface. The evolved protein expresses well in bacteria and binds to TfR with a dissociation constant of approximately 1 μM, as measured using an SPR assay. In addition, we showed that a TB08 S3.1–GFP variant was internalized within HeLa cells, indicating that the evolved protein allows for the delivery of sGFP-size cargo, showing potential for biomedical delivery applications. The small size of the designed protein (80 amino acids), different binding mode compared with

17424658, 2022, 10, Downloaded from https://febs.onlinelibrary.wiley.com/doi/10.1111/febs.16311 by Elena Ambrosetti - Cochraneltalia , Wiley Online Library on [08/11/2025]. See the Terms and Conditions (https://onlinelibrary.wiley.com/terms-and-conditions) on Wiley Online Library for rules of use; OA articles are governed by the applicable Creative Commons License

antibodies or existing miniproteins, and robustness to modifications, provides an alternative to other currently available TfR-mediated delivery systems.

Materials and methods

Computational protein design

ROSETTA computational software [31] was used to design and optimize protein binders by taking the advantage of naturally occurring interactions and building these into preexisting small protein scaffolds. HFE binds TfR with hotspot residues V78 and W81 [32]. The helical segments containing the valine and tryptophane hotspot residues was swapped with same length helical fragments in a protein scaffold (Fig. S1). The length of the native α-helix from HFE, according to its complexed structure with TfR, PDB id 1de4 [11], was varied to include each of the following helical segments: 25 (LQLSQSLKGWDHMFTVDFWTIMENH), 23 (LQLSQSLKGWDHMFTVDFWTIME), 19 (QSLKGWD HMFTVDFWTIME), and 16 (KGWDHMFTVDFW TIME) with the hotspot residues denoted in bold in the amino acid sequence. The helical segments were generated by trying to retain as many interactions as possible along the binding surface with the target receptor while deleting the residues that point toward the opposite direction into the protein core. The truncations correspond to approximately one helical turn with the crystal structure atom coordinates without any optimization. The protein scaffold list that was used for the grafting procedure was assembled from the PDB according to the following criteria: (a) 40–120 amino acids long, (b) at least one α-helix, (c) less than 99% sequence homology to the other proteins in the set, (d) resolution lower than 3.0 Å, (e) R-factor lower than 1.0, (f) no nucleic acids bound, and (g) non-canonical amino acids converted to their closest canonical form. This resulted in approximately 1000 scaffolds used for the computational design for each of the HFE segments. The grafting and the sequence optimization was carried out by ROSETTA with the RosettaScripts application using the MotifGraft mover [33]. The grafted helix in a scaffold retained the native HFE residues including the hotspots forming the protein–protein interface surface with the TfR and necessitated redesign of the helix part involved in forming the protein core. The native scaffold amino acids were favored either by receiving a lower energy offset or by scaling the propensities within the position-specific scoring matrix (PSSM) derived from homologues. The solutions with grafted helix in different redesigned and structurally optimized scaffolds were sorted according to shape complementarity and surface area followed by visual inspection of the top ranked solutions. Additionally, sequence optimization was carried out by RosettaRemodel application [26]. The genes were ordered with overhanging homologues ends to match overlapping ends of the yeast display plasmid, pETCON [22].

Flow cytometry analysis of yeast surface displayed variants

The genes encoding for the designs were ordered from IDT (Integrated DNA Technologies, USA). The linear pETCON [22] plasmid, cleaved with FastDigest *Nde*I and *Xho*I (Thermo Scientific, USA) and a corresponding gene were used to construct the expression vectors by homologous recombination in *S. cerevisiae* EBY100 strain. The transformation of yeast cells was performed by heat shock procedure described in Gietz and Schiestl [34], with selection on agar plates made with C–UT growth medium. The C–UT medium was prepared as follows: 1.85 $g{\cdot}L^{-1}$ synthetic complete mixture, Kaiser, drop-out *–Trp –Ura* (Formedium, England), 6.9 $g{\cdot}L^{-1}$ yeast nitrogen base without amino acids with ammonium sulphate (Formedium, England), and 20 $g{\cdot}L^{-1}$ d-(+)-glucose (Sigma–Aldrich, USA). The cloning was confirmed by sequencing after colony PCR. Each colony was dissolved in 20 µL reaction containing 5 $mg{\cdot}mL^{-1}$ zymolase (Seikagaku corporation, Japan), 250 mM HEPES, 2 M sorbitol, and 15% glycerol, and incubated for 1 h at 37 °C in adaptation of the protocol from Singh *et al.* [35]. Two microliters of the zymolase reaction was subjected to 30 cycles of PCR amplification with the forward primer CCATACGACGTTCCAGACTACG and reverse primer CTATTACAAGTCCTCTTCAGAA. After PCR clean-up with ExoSAP-IT (Thermo Fisher Scientific, USA), one of the primers was added to the Mix2Seq kit (EuroFins, Germany) for sequencing. For plasmid purification, cells were lysed with zymolase, from 10 mL of yeast cells, grown on to OD_{600} = 6 in C–UT growth medium. QIAprep spin Miniprep Kit (Qiagen, Germany) was used to extract the plasmid.

Yeast surface display (YSD) method [36] was used to experimentally assay the binding of designed variants to TfR. With YSD, we monitored both the expression of the designed proteins on the yeast cell surface and the binding to the target receptor. For the binding assay, the avi-tagged TfR was expressed and purified from HEK293f or Expi293f cells and subsequently biotinylated according to the protocols published in Sjöström *et al.* [37]. The transformed EBY100 yeast cells were passaged overnight in C–UT medium, and protein surface expression was induced by pelleting cells at 5000 × ***g*** for 5 min, resuspending them in C–UT medium containing galactose instead of glucose at the final density of OD_{600} = 0.75 and incubating for 20 h at 180 r.p.m. at 20 °C. Fifty microliters of induced cells were washed with 100 µL PBSF (8 g NaCl, 0.2 g KCl, 1.44 g Na_2HPO_4, 0.24 g KH_2PO_4, and 1 g BSA in 1 L deionized sterile filtered H_2O, adjusted to pH 7.4) and labeled with TfR for 1.5 h on ice, in 50 µL PBSF, or, for lower concentrations of TfR, in a volume resulting in at least 10 times

17424658, 2022, 10, Downloaded from https://febs.onlinelibrary.wiley.com/doi/10.1111/febs.16311 by Elena Ambrosetti - CochraneItalia , Wiley Online Library on [08/11/2025]. See the Terms and Conditions (https://onlinelibrary.wiley.com/terms-and-conditions) on Wiley Online Library for rules of use; OA articles are governed by the applicable Creative Commons License

more TfR than the approximate number of surface-expressed molecules. After another wash with PBSF, the cells were labeled on ice, in dark for 30 min with 50 μL 1 : 100 diluted chicken anti c-Myc FITC conjugated antibody and 1 : 20 SAPE in PBSF. The cells were washed with PBSF and spun down, before dissolving cell pellet in PBSF and measuring 50 000 single yeast cells with a BD Accuri C6 flow cytometer with a blue (488 nm) laser for excitation and the bandpass filters 533/30 and 585/40 for detecting FITC and SAPE fluorescence, respectively.

Selection of variants with improved binding

pETCON containing a gene of interest was used for random mutagenesis (Mutazyme II kit, Stratagene, USA) with the sequencing primers above to generate the library of TB08dm variants. Two reactions were set up with either 5 ng or 500 ng insert to titrate the number of mutations per gene. Both samples were transformed into yeast cells by electroporation in 0.2 cm cuvettes (Bio-Rad, USA), with 1 μg pETCON, 3 μg TB08dm in 100 μL following the published protocol [38] with 0.1 M LiAc (Sigma-Aldrich, USA) and 10 mM DTT (Fisher Bioreagents, USA) for conditioning of cells. The electroporated cells were transferred into 10 mL of a 1 : 1 mix of 2 M sorbitol and YPD medium [20 $g{\cdot}L^{-1}$ peptone (Nordic biolabs, Sweden), 10 $g{\cdot}L^{-1}$ yeast extract (Sigma–Aldrich, USA), 20 $g{\cdot}L^{-1}$ d-(+)-glucose (Sigma–Aldrich, USA)] and incubated at 30 °C at 180 r.p.m. for 1 h. The cells were collected and resuspended in 50 mL C–UT medium, and the number of transformants was determined by plating 5 μL and 50 μL of the culture on selective C–UT agar plates. After incubation at 30 °C for two days, colony-forming units were counted to calculate the size of the mutagenesis library. Errors per gene were determined based on the alignment with the native gene after DNA sequencing with Mix2Seq kit (EuroFins, Germany).

Fluorescence-activated cell sorting (FACS) in combination with the YSD method [36] had been used to select variants with improved binding signal to the target receptor. In brief, EBY100 yeast cells were passaged overnight in C–UT medium, and protein surface expression was induced by changing to C–UT medium containing galactose instead of glucose and incubating at 20 °C shaking at 180 r.p.m. Five hundred microliters of induced cells OD_{600} = 0.75 were washed with 1 mL PBSF and, thereafter, labeled on ice for 1.5 h at 1 μM TfR in 500 μL PBSF. Cell were pelleted at 5000 × ***g*** for 5 min. With samples kept on ice until measurement, another wash with 1 mL PBSF was performed before 30 min of labeling with 1 : 100 diluted chicken anti-cmyc-FITC-conjugated antibody that monitored yeast surface protein expression (Immunology Consultants Laboratory, USA) and 1 : 20 SAPE (Streptavidin–R-Phycoerythrin Conjugate; Invitrogen, USA) that detected biotinylated TfR binding to yeast expressed protein in 500 μL PBSF. The cells were washed with PBSF, pelleted, and kept on ice until sorting with a Biorad S3e. Excitation was done with a 488 nm blue laser, and the bandpass filters used to detect SAPE and FITC fluorescence were 586/25 and 525/30, respectively. Cells were resuspended in PBSF, gated on the top 5% in the first sort and top 1% of cells in subsequent rounds of FACS, in a triangular gate on the diagonal top left of the FITC/SAPE-positive population. Cells were collected in C–UT supplemented with penicillin and streptomycin. Between each round of FACS, the cells were passaged twice in 50 mL C–UT medium. Determination of apparent binding affinity by YSD titration was performed following the protocol published in Sjöström *et al.* [37]. Flow cytometry figures were prepared using FLOWJO software [39].

In vitro Surface Plasmon Resonance (SPR)-binding assay

To perform *in vitro* binding characterization, variants were cloned in pET29b(+) vector at *Nde*I and *Xho*I restriction sites and confirmed by sequencing (Mix2Seq kit, Eurofins). *E. coli* Tuner (DE3) competent cells (Invitrogen) were chemically transformed and used for the protein expression. A culture of 0.5 L of LB was inoculated and grown shaking at 180 r.p.m., 37 °C to OD600 = 0.6; the temperature was lowered to 20 °C and the protein expression was induced by 0.2 mM IPTG for ~ 18 h. Cells were collected at 5000 × *g* for 20 min; the cell pellet was dissolved in 25 mL buffer (25 mM HEPES, 100 mM NaCl, pH 7.4) and sonicated five times at 40% amplitude for 20/20 s on/off. Lysed cells were centrifuged at 10 000 × ***g*** for 30 min. Supernatant was filtered through a 0.22 μm filter and loaded on a HisPur Cobalt resin column (Thermo Scientific), preequilibrated with 25 mM HEPES, 100 mM NaCl, pH 7.4. The column was washed with 25 mM HEPES, 100 mM NaCl, 10 mM imidazole, pH 7.4, and eluted with 25 mM HEPES, 100 mM NaCl, 150 mM imidazole, pH 7.4.

The gene encoding for sGFP [40] was synthetized (Integrated DNA Technologies, USA) C-terminally from the TB08 S3.1 gene sequence with a GSAGSAAGSEF linker in between according to the tagging procedure outlined in Ref. [40]. The TB08 S3.1–sGFP-tagged variant and sGFP alone was cloned into pET29b(+) plasmid at the *Nde*I and *Xho*I restrictions sites and confirmed by sequencing (Mix2-Seq kit, EuroFins) with both T7 forward and T7 reverse primers, respectively. The PDB id 3zzp protein scaffold was genetically fused to sGFP according to the TB08 S3.1–sGFP variant, synthetized and ligated in between *Nde* I/*Xho* I sites of pET29b(+) vector (Genscript). For the protein purification of TB08 S3.1–sGFP, 3zzp–sGFP, and sGFP, the plasmids were transformed into *E. coli* Tuner cells, expressed, and purified as above for the untagged variant. The protein expression was confirmed by SDS–PAGE or FPLC size exclusion chromatography (SEC) over HiLoad 16/60 Sephacryl 100 column.

17424658, 2022, 10, Downloaded from https://febs.onlinelibrary.wiley.com/doi/10.1111/febs.16311 by Elena Ambrosetti - CochraneItalia , Wiley Online Library on [08/11/2025]. See the Terms and Conditions (https://onlinelibrary.wiley.com/terms-and-conditions) on Wiley Online Library for rules of use; OA articles are governed by the applicable Creative Commons License

For recording circular dichroism (CD) spectra and temperature stability measurement scans, J-815 spectrometer (JASCO) was used. Proteins in the HEPES buffer were buffer exchanged over a PD–10 column into 10 mM potassium buffer, 100 mM KF, pH = 7.4, and diluted to 0.1 mg·mL^{-1}. CD scans were recorded between 195 and 250 nm at 1 nm interval, and temperature scans were determined between 15 and 90 °C at 220 nm wavelength.

Binding of protein variants (TB08, TB08 S3.1, and TB08 S3.1–sGFP) was determined by SPR experiments, using a Biacore T200 instrument (Cytiva). Biotinylated TfR was immobilized to streptavidin (SA) sensor chip (Cytiva). In addition, either TfR or Her3 was immobilized by amine-coupling reactions on a CM5 sensor chip (Cytiva), according to the manufacturer's instructions. To determine the dissociation equilibrium constant (K_d), the association rate constant (k_{on}), and dissociation rate constant (k_{off}), standard kinetic tests were performed by injecting different concentrations of proteins (TB08, TB08 S3.1, and TB08 S3.1–sGFP) in HBS-P+ (HEPES 10 mM, NaCl 150 mM, p20 0.05%) running buffer (Cytiva). The protein concentrations tested on the SA chip were 0.63, 1.25, 2.5, 5, and 10 μM; protein concentrations tested on CM5 chip were 6, 8.8, 13.3, 20, and 30 μM for TB08 and 1.25, 2.5, 5, 10, and 20 μM for TB08 S3.1. The injection of each concentration was performed using an association phase of 150 s and a dissociation phase of 300 s. The kinetic parameters were determined using the BIAEVALUATION 3.0 software, assuming a 1 : 1 binding model. Binding of transferrin was verified by flows of increasing concentrations of transferrin (6.2, 18.5, 55.5, 166.7, and 500 nM) in single-cycle kinetic mode (association phase of 120 s and a dissociation phase of 300 s) over a SA chip sensor surface with immobilized biotinylated TfR.

HeLa cell culture, flow cytometry, and microscopy analysis

The human epithelial HeLa cell line was cultured in Dulbecco′s modified Eagle′s medium (DMEM) without phenol red (Gibco) supplemented with 10% fetal bovine serum, Glutamax (Invitrogen), penicillin, and 100 μg·mL^{-1} streptomycin at 37 °C under a humified 5% CO_2 atmosphere and subcultured when confluent (chemicals from Sigma–Aldrich). For flow cytometry, HeLa cells were seeded on six-well plates, 4×10^5 cells/well, and allowed to grow for 48 h. Cell culture medium was removed, cells were rinsed twice with phosphate buffered saline (PBS, Sigma–Aldrich), and the confluent cells were incubated with fluorescently labeled proteins diluted in cell culture medium at their labeling concentrations, for 2 h and 30 min at 4 °C or 37 °C. Cells in PBS alone were used as a negative control. Plates with cells were rotated three times during the labeling process.

For cell labeling, human holo-Tf (T0665, Sigma–Aldrich, USA) was modified with Pierce FITC Antibody Labeling Kit (Thermo Scientific, USA) according to the manufacturer's standard protocol, which resulted in labeling ratio of 1.2 : 1 of FITC : Tf. HeLa cells were mechanically detached from the plate and washed twice (100 × *g*, 2 min) with PBS before flow cytometry measurement (BD Accuri C6), using a 480 nm blue laser for excitation and 533/30 filter for detection.

For microscopy analysis, HeLa cells were seeded at a density of 15×10^3 in eight-well chamber glass slides, Laboratory-TEK Chamber slide system™ (Thermo Fisher Scientific) and allowed to grow for 48 h. Prior to the microscopy analysis, labeled HeLa cells were washed three times with PBS, fixed with ice cold 4% paraformaldehyde in phosphate buffer (Sigma-Aldrich), in the dark, at room temperature, for 10 min, and washed three times with PBS. Cells were thereafter either left unstained or stained for F-actin with Phalloidin-tetramethylrhodamine isothiocyanate (TRITC) (Thermo Fisher Scientific) 1 : 100, during 10 min at room temperature, for actin visualization. Stained cells were thereafter washed with three times in PBS and mounted with anti-fading mounting medium Vectashield with or without 4′,6-diamidino-2-phenylindole (DAPI) (Vector Laboratories Burlingame, CA, USA). Images were captured with Nikon epifluorescence microscope (Nikon, Tokyo, Japan) using Nis-element imaging (version 4.3, Nikon) or by using a confocal microscope (Nikon) EZ-C1 2.20 software. Pictures were bright adjusted in ADOBE Photoshop version 21.2.3.

Acknowledgements

We thank Associate Prof. Ingemar André at Lund University for the use of BioRad S3 cell sorter, Elaf Taleb, Leonard Sparring, and Leila Lahchaichi for their contributions in cloning, generating libraries, and with flow cytometry analysis, and Juni Andréll for helping with TfR purification. SB is grateful for financial support from Vinnova (2015-04912) and FHL. AIT acknowledges funding from the Knut and Alice Wallenberg Foundation (2017.0114). The computations were enabled by resources provided by SNIC at Lunarc partially funded by the Swedish Research Council through grant agreement no. SNIC 2019/3-320.

Conflict of interest

The authors declare no conflict of interest.

Author contributions

DS and SB designed the study. DS did the cloning, generated libraries, and analyzed the evolved mutants with flow cytometry. SJG purified TfR. DS and SB analyzed the data. CM performed microscopy. EA and

17424658, 2022, 10, Downloaded from https://febs.onlinelibrary.wiley.com/doi/10.1111/febs.16311 by Elena Ambrosetti - Cochraneltalia , Wiley Online Library on [08/11/2025]. See the Terms and Conditions (https://onlinelibrary.wiley.com/terms-and-conditions) on Wiley Online Library for rules of use; OA articles are governed by the applicable Creative Commons License

AIT planned SPR measurements, which were performed and analyzed by EA. SB supervised the study. DS and SB wrote the manuscript with input from all co-authors.

Data availability statement

Scripts available within the supplementary material; otherwise data available on request from the authors.

References

1 Andrews NC & Schmidt PJ (2007) Iron homeostasis. *Annu Rev Physiol* **69**, 69–85.
2 Eckenroth BE, Steere AN, Chasteen ND, Everse SJ & Mason AB (2011) How the binding of human transferrin primes the transferrin receptor potentiating iron release at endosomal pH. *Proc Natl Acad Sci USA* **108**, 13089–13094.
3 Kariolis MS, Wells RC, Getz JA, Kwan W, Mahon CS, Tong R, Kim DJ, Srivastava A, Bedard C, Henne KR *et al.* (2020) Brain delivery of therapeutic proteins using an Fc fragment blood-brain barrier transport vehicle in mice and monkeys. *Sci Transl Med* **12**, 43.
4 Lee JH, Engler JA, Collawn JF & Moore BA (2001) Receptor mediated uptake of peptides that bind the human transferrin receptor. *Eur J Biochem* **268**, 2004–2012.
5 Meister SW, Hjelm LC, Dannemeyer M, Tegel H, Lindberg H, Stahl S & Lofblom J (2020) An affibody molecule is actively transported into the cerebrospinal fluid via binding to the transferrin receptor. *Int J Mol Sci* **21**, 81.
6 Sahtoe DD, Coscia A, Mustafaoglu N, Miller LM, Olal D, Vulovic I, Yu TY, Goreshnik I, Lin YR, Clark L *et al.* (2021) Transferrin receptor targeting by de novo sheet extension. *Proc Natl Acad Sci USA* **118**, 77.
7 Wiley DT, Webster P, Gale A & Davis ME (2013) Transcytosis and brain uptake of transferrin-containing nanoparticles by tuning avidity to transferrin receptor. *Proc Natl Acad Sci USA* **110**, 8662–8667.
8 Yu YJ, Atwal JK, Zhang Y, Tong RK, Wildsmith KR, Tan C, Bien-Ly N, Hersom M, Maloney JA, Meilandt WJ *et al.* (2014) Therapeutic bispecific antibodies cross the blood-brain barrier in nonhuman primates. *Sci Transl Med* **6**, 261.
9 Testi C, Boffi A & Montemiglio LC (2019) Structural analysis of the transferrin receptor multifaceted ligand (s) interface. *Biophys Chem* **254**, 106242.
10 Cheng Y, Zak O, Aisen P, Harrison SC & Walz T (2004) Structure of the human transferrin receptor-transferrin complex. *Cell* **116**, 565–576.
11 Bennett MJ, Lebrón JA & Bjorkman PJ (2000) Crystal structure of the hereditary haemochromatosis protein HFE complexed with transferrin receptor. *Nature* **403**, 46–53.
12 Giannetti AM & Bjorkman PJ (2004) HFE and transferrin directly compete for transferrin receptor in solution and at the cell surface. *J Biol Chem* **279**, 25866–25875.
13 West AP Jr, Giannetti AM, Herr AB, Bennett MJ, Nangiana JS, Pierce JR, Weiner LP, Snow PM & Bjorkman PJ (2001) Mutational analysis of the transferrin receptor reveals overlapping HFE and transferrin binding sites. *J Mol Biol* **313**, 385–397.
14 Liu AP, Aguet F, Danuser G & Schmid SL (2010) Local clustering of transferrin receptors promotes clathrin-coated pit initiation. *J Cell Biol* **191**, 1381–1393.
15 Abraham J, Corbett KD, Farzan M, Choe H & Harrison SC (2010) Structural basis for receptor recognition by New World hemorrhagic fever arenaviruses. *Nat Struct Mol Biol* **17**, 438–444.
16 Gruszczyk J, Huang RK, Chan LJ, Menant S, Hong C, Murphy JM, Mok YF, Griffin MDW, Pearson RD, Wong W *et al.* (2018) Cryo-EM structure of an essential Plasmodium vivax invasion complex. *Nature* **559**, 135–139.
17 Montemiglio LC, Testi C, Ceci P, Falvo E, Pitea M, Savino C, Arcovito A, Peruzzi G, Baiocco P, Mancia F *et al.* (2019) Cryo-EM structure of the human ferritin-transferrin receptor 1 complex. *Nat Commun* **10**, 1121.
18 Terstappen GC, Meyer AH, Bell RD & Zhang W (2021) Strategies for delivering therapeutics across the blood-brain barrier. *Nat Rev Drug Discov* **20**, 362–383
19 Johnsen KB, Bak M, Kempen PJ, Melander F, Burkhart A, Thomsen MS, Nielsen MS, Moos T & Andresen TL (2018) Antibody affinity and valency impact brain uptake of transferrin receptor-targeted gold nanoparticles. *Theranostics* **8**, 3416–3436.
20 Cohen-Dvashi H, Amon R, Agans KN, Cross RW, Borenstein-Katz A, Mateo M, Baize S, Padler-Karavani V, Geisbert TW & Diskin R (2020) Rational design of universal immunotherapy for TfR1-tropic arenaviruses. *Nat Commun* **11**, 67.
21 Sjöström DJ, Berger SA, Oberdorfer G & Bjelic S (2020) Computational backbone design enables soluble engineering of transferrin receptor apical domain. *Proteins* **88**, 1569–1577.
22 Fleishman SJ, Whitehead TA, Ekiert DC, Dreyfus C, Corn JE, Strauch EM, Wilson IA & Baker D (2011) Computational design of proteins targeting the conserved stem region of influenza hemagglutinin. *Science* **332**, 816–821.
23 Procko E, Berguig GY, Shen BW, Song Y, Frayo S, Convertine AJ, Margineantu D, Booth G, Correia BE, Cheng Y *et al.* (2014) A computationally designed inhibitor of an Epstein-Barr viral Bcl-2 protein induces apoptosis in infected cells. *Cell* **157**, 1644–1656.
24 Azoitei ML, Correia BE, Ban YE, Carrico C, Kalyuzhniy O, Chen L, Schroeter A, Huang PS, McLellan JS, Kwong PD *et al.* (2011) Computation-guided backbone grafting of a discontinuous motif onto a protein scaffold. *Science* **334**, 373–376.

17424658, 2022, 10, Downloaded from https://febs.onlinelibrary.wiley.com/doi/10.1111/febs.16311 by Elena Ambrosetti - CochraneItalia , Wiley Online Library on [08/11/2025]. See the Terms and Conditions (https://onlinelibrary.wiley.com/terms-and-conditions) on Wiley Online Library for rules of use; OA articles are governed by the applicable Creative Commons License

25 Haglund E, Danielsson J, Kadhirvel S, Lindberg MO, Logan DT & Oliveberg M (2012) Trimming down a protein structure to its bare foldons: spatial organization of the cooperative unit. *J Biol Chem* **287**, 2731–2738.
26 Huang PS, Ban YE, Richter F, Andre I, Vernon R, Schief WR & Baker D (2011) RosettaRemodel: a generalized framework for flexible backbone protein design. *PLoS One* **6**, e24109.
27 Yu YJ, Zhang Y, Kenrick M, Hoyte K, Luk W, Lu Y, Atwal J, Elliott JM, Prabhu S, Watts RJ *et al.* (2011) Boosting brain uptake of a therapeutic antibody by reducing its affinity for a transcytosis target. *Sci Transl Med* **3**, 84.
28 Bridges KR & Smith BR (1985) Discordance between transferrin receptor expression and susceptibility to lysis by natural killer cells. *J Clin Invest* **76**, 913–918.
29 Mitchell DJ, Kim DT, Steinman L, Fathman CG & Rothbard JB (2000) Polyarginine enters cells more efficiently than other polycationic homopolymers. *J Pept Res* **56**, 318–325.
30 Thoren PE, Persson D, Isakson P, Goksor M, Onfelt A & Norden B (2003) Uptake of analogs of penetratin, Tat(48–60) and oligoarginine in live cells. *Biochem Biophys Res Commun* **307**, 100–107.
31 Leaver-Fay A, Tyka M, Lewis SM, Lange OF, Thompson J, Jacak R, Kaufman K, Renfrew PD, Smith CA, Sheffler W *et al.* (2011) ROSETTA3: an object-oriented software suite for the simulation and design of macromolecules. *Methods Enzymol* **487**, 545–574.
32 Lebron JA & Bjorkman PJ (1999) The transferrin receptor binding site on HFE, the class I MHC-related protein mutated in hereditary hemochromatosis. *J Mol Biol* **289**, 1109–1118.
33 Fleishman SJ, Leaver-Fay A, Corn JE, Strauch EM, Khare SD, Koga N, Ashworth J, Murphy P, Richter F, Lemmon G *et al.* (2011) RosettaScripts: a scripting language interface to the Rosetta macromolecular modeling suite. *PLoS One* **6**, e20161.
34 Gietz RD & Schiestl RH (2007) Frozen competent yeast cells that can be transformed with high efficiency using the LiAc/SS carrier DNA/PEG method. *Nat Protoc* **2**, 1–4.
35 Singh MV & Weil PA (2002) A method for plasmid purification directly from yeast. *Anal Biochem* **307**, 13–17.
36 Chao G, Lau WL, Hackel BJ, Sazinsky SL, Lippow SM & Wittrup KD (2006) Isolating and engineering human antibodies using yeast surface display. *Nat Protoc* **1**, 755–768.
37 Sjöström DJ, Lundgren A, Garforth SJ & Bjelic S (2021) Tuning the binding interface between Machupo virus glycoprotein and human transferrin receptor. *Proteins* **89**, 311–321.
38 Benatuil L, Perez JM, Belk J & Hsieh CM (2010) An improved yeast transformation method for the generation of very large human antibody libraries. *Protein Eng Des Sel* **23**, 155–159.
39 FlowJo (2019) FlowJo™ Software Version 10.5.0. in Ashland, OR: Becton, Dickinson and Company.
40 Pedelacq JD, Cabantous S, Tran T, Terwilliger TC & Waldo GS (2006) Engineering and characterization of a superfolder green fluorescent protein. *Nat Biotechnol* **24**, 79–88.

Supporting information

Additional supporting information may be found online in the Supporting Information section at the end of the article.

Table S1. Summary of the mean fluorescence units (MFU) values reported for the YSD figures.

Fig. S1. Computational methodology used for protein design.

Fig. S2. Yeast surface display of TB08 and TB08dm variants.

Fig. S3. SPR measurements of transferrin binding to TfR.

Fig. S4. Binding affinity characterization by *in vitro* SPR assay and YSD titration.

Fig. S5. SPR measurements of TB08 and TB08 S3.1 variants with Her3.

Fig. S6. Competition assay of yeast-displayed TB08 S3.1 with transferrin binding to TfR.

Fig. S7. Competition assay with TfR between TB08 S3.1 and yeast-displayed TB08 S3.1.

Fig. S8. Circular dichroism of TB08 and TB08 S3.1; affinity purification and gel filtration of TB08 S3.1–sGFP.

Fig. S9. Representative confocal microscopy images of HeLa cells with TB08 S3.1–sGFP and labeled with phalloidin–TRITC.

Fig. S10. Representative confocal microscopy images of HeLa cells with Tf-FITC and labeled with phalloidin–TRITC.

Fig. S11. Temperature dependence of cellular protein uptake with Tf-FITC or TB08 S3.1¬–sGFP.

Fig. S12. Titration of HeLa cells with TB08 S3.1–sGFP.

Fig. S13. Negative controls sGFP alone and coupled to the original scaffold used for design, PDB ID 3zzp, and comparison of sGFP, 3zzp–sGFP, and TB08 S3.1–sGFP binding at 400 nM.

17424658, 2022, 10, Downloaded from https://febs.onlinelibrary.wiley.com/doi/10.1111/febs.16311 by Elena Ambrosetti - Cochraneltalia , Wiley Online Library on [08/11/2025]. See the Terms and Conditions (https://onlinelibrary.wiley.com/terms-and-conditions) on Wiley Online Library for rules of use; OA articles are governed by the applicable Creative Commons License